EPJ Web of Conferences **73**, 04005 (2014)
DOI: 10.1051/epjconf/20147304005

Measurement of the double polarization observable E in η'-photoproduction

Farah Noreen Afzal[a] for the CBELSA/TAPS collaboration

Helmholtz-Institut für Strahlen- und Kernphysik, University of Bonn, Nussallee 14-16, 53115 Bonn, Germany

Abstract. The nucleon excitation spectrum is investigated at the Crystal Barrel experiment through different photoproduction reactions. The photoproduction of single η' mesons off protons is of particular importance since it offers the opportunity to study the high-lying resonances and therefore the part of the nucleon excitation spectrum where many missing resonances are predicted. Preliminary results of the double polarization observable E and the decomposition of the total cross section into its helicity-dependent components $\sigma_{1/2}$ and $\sigma_{3/2}$ in η'-photoproduction are presented for beam energies from 1450 MeV to 2320 MeV.

1. Introduction

Precise knowledge of the nucleon excitation spectra provides information about the dynamics inside the nucleon and the according relevant degrees of freedom. Since baryon resonances have large widths, many resonances with different spin-parities overlap, making it difficult to investigate individual states. In order to deconvolve the spectrum and extract resonance properties, partial wave analyses need to be performed. In the past, mainly πN- elastic scattering data was used for this purpose. Meson photoproductions off nucleons provide an important alternative tool to investigate baryon resonances, especially the ones that couple weakly to the πN- channel. The study of η'-photoproduction in particular offers exclusive access to N^* resonances with isospin $I = 1/2$ as opposed to π^0-photoproduction. Furthermore, the high mass of η' allows to explore the high mass region ($m_{N^*} > 1890$ MeV) of the nucleon excitation spectrum, where various model calculations, that have been conducted in the past [1, 2], predict more excited states than there have been measured so far.

During the last decade, first differential cross section data in η'-photoproduction have been published by the CBELSA/TAPS [3] and the CLAS [4] collaborations. For a unique partial wave solution however, additional single and double polarization observables need to be measured [5]. Using a circularly polarized photon beam in combination with a longitudinally polarized target gives access to the double polarization observable E. It describes the asymmetry between the two possible helicity states $h = 1/2$

[a]e-mail: afzal@hiskp.uni-bonn.de

and $h = 3/2$, where the spins of the beam photon and the target proton are either anti-aligned or aligned:

$$\mathrm{E} = \frac{\sigma_{1/2} - \sigma_{3/2}}{\sigma_{1/2} + \sigma_{3/2}} \,. \tag{1}$$

Here, $\sigma_{1/2}$ and $\sigma_{3/2}$ denote the helicity-dependent cross sections, that can be written as $\sigma_{1/2(3/2)} = \sigma_0[1 \,{}_{(\pm)}\, p_T\, p_\odot \mathrm{E}]$ with the unpolarized cross section σ_0 and the target and the beam polarization degrees, p_T and $p_\odot$, respectively.

2. Experimental setup

The presented data was obtained with the Crystal Barrel/TAPS experiment located at the electron stretcher accelerator ELSA in Bonn. For the measurement of the double polarization observable E, a circularly polarized photon beam was acquired by passing a 2.4 GeV beam of longitudinally polarized electrons through a bremsstrahlung radiator. The resulting photon beam had a polarization degree of up to $p_\odot \leq 60\%$ which was determined with the help of a Møller polarimeter. In order to determine the energy of the bremsstrahlung photons, the electrons were deflected by a dipole magnet momentum dependent into a tagging hodoscope consisting of scintillating fibers and bars. The photon beam impinged on the frozen-spin butanol (C_4H_9OH) target with an average polarization degree of $p_T \approx 71\%$. For the detection of neutral mesons decaying into photons in the final state, the main component of the experimental setup consisted of two calorimeters, the CsI(Tl) Crystal Barrel and the BaF_2 MiniTAPS detectors. Combined, both detectors allowed energy and direction measurements of photons for almost the full 4π solid angle. The three-layered scintillating detector surrounding the target and the plastic scintillation counters mounted in front of the Crystal Barrel's forward and the MiniTAPS detector's crystals enabled the identification of charged particles.

3. Event selection

For the selection of possible $\gamma p \to \eta' p$ events, the two neutral decay modes of η': $\eta' \to \gamma\gamma$ (BR: 2.22%) and $\eta' \to \pi^0\pi^0\eta \to 6\gamma$ (BR: 8.6%) were used.

The reaction $\gamma p \to \eta' p \to \gamma\gamma p$ was reconstructed by considering only events with three distinct hits in the calorimeters, two from the photons and one from the proton, and applying kinematic cuts to these events. The η' four-momentum could be reconstructed from the four-momenta of the two photons. A $\pm 3\sigma$ cut was applied on the $\gamma\gamma$-invariant mass around the η' mass (compare Fig. 1). The proton however was identified using the missing mass of the system $\gamma p \to \eta' X$ as the protons were not always contained completely in the calorimeters. The missing mass had to be in agreement with the PDG proton mass within 3σ. Furthermore, the polar angle θ of the proton calculated from the missing mass and the measured proton had to be consistent within $\pm 11^\circ$. Since the combined transverse momentum of proton and η' had to vanish, a cut to the azimuthal angle Φ was used as well (coplanarity: $162^\circ < \Phi_p - \Phi_{\eta'} < 198^\circ$). Additionally, the energy of the beam photons was calculated using the kinematics of the reaction. Events with a calculated beam energy above the photoproduction threshold of η' ($E_\gamma = 1447\,\mathrm{MeV}$) were retained. Lastly, time coincidence of the beam photons and the reaction products was demanded.

In order to reconstruct the reaction $\gamma p \to \eta' p \to 2\pi^0\eta p \to 6\gamma p$, events with six photons and one proton were selected. The six decay photons were combined pairwise to $2\pi^0\eta$ and the combinatorial background was reduced by applying $\pm 3\sigma$ cuts on the $\gamma\gamma$-invariant masses around the π^0 and η masses. Then a kinematic fit with the hypothesis $\gamma p \to 2\pi^0\eta p$ was performed. Thereby, a measured proton was not required. Instead the proton was calculated using energy and momentum conservation. Only if the confidence level of the fit result was higher than 0.1, the events were retained. In order to reduce contributions from the main background channel $\gamma p \to 3\pi^0 p$, a kinematic fit with the hypothesis

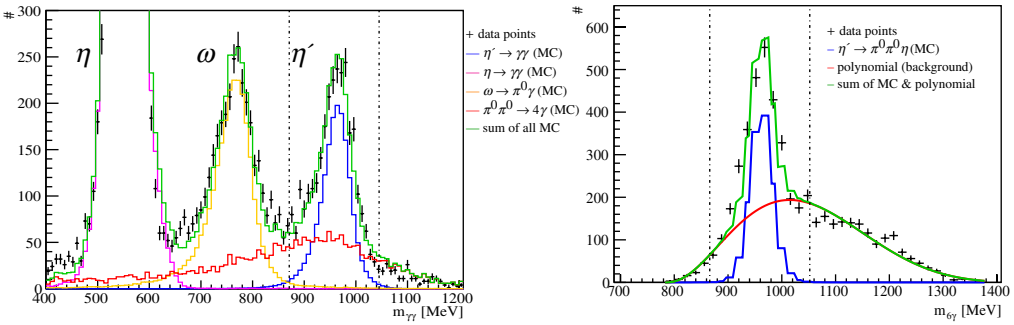

Figure 1. The invariant mass spectra for both decay modes: $\eta' \to \gamma\gamma$ and $\eta' \to \pi^0\pi^0\eta \to 6\gamma$.

$\gamma p \to 3\pi^0 p$ was performed as well and an anti-cut was applied by rejecting all events that had a confidence level higher than 0.1 for this hypothesis. The 6γ-invariant mass was calculated and a $\pm 3\sigma$ cut was applied around the η' mass (compare Fig. 1). Additionally, selected events had to fulfill the same criteria as described for the other decay mode regarding the missing mass, coplanarity, calculated beam photon energy and time coincidence.

Figure 1 shows the $\gamma\gamma$-invariant mass on the left and the 6γ-invariant mass on the right. In both decay modes, non-negligible background contributions remained that could not be reduced through further kinematic cuts. In the case of $\eta' \to \gamma\gamma$, the main background contribution is due to the $2\pi^0$-photoproduction channel. It was estimated and subtracted using Monte Carlo events. For the $\eta' \to 6\gamma$ case, the background consists most probably of a mixture of combinatorial background and of $3\pi^0$-, $\pi^0\omega$- and $2\pi^0\eta$-photoproduction channel contributions. The background was fitted by a polynomial function and subtracted. Since the background was polarized for both decay modes, the background needed to be subtracted separately for both helicity $h = 1/2$ and $h = 3/2$ states.

4. Extraction of the double polarization observable E

Using the definition of the helicity-dependent cross sections and Eq. (1), leads to:

$$\mathrm{E} = \frac{N_{1/2} - N_{3/2}}{N_{1/2} + N_{3/2}} \cdot \frac{1}{d} \frac{1}{p_T\, p_\odot}, \tag{2}$$

where $N_{1/2}$ and $N_{3/2}$ are the helicity-dependent count rates, d the dilution factor and $p_T\, p_\odot$ the target and beam polarization degrees. As the data was obtained with a butanol (C_4H_9OH) target, not only the polarizable free protons in hydrogen nuclei, but also the unpolarized bound nucleons in carbon and oxygen nuclei contribute to the count rates. The dilution factor, which specifies the amount of polarizable free protons in the selected data ($d = N_{\mathrm{free}}/(N_{\mathrm{free}} + N_{\mathrm{bound}})$), takes this into account. It was determined by using an additional data set which was taken with a carbon foam target and scaling the coplanarity distribution of the carbon data (N_C) to the one of the butanol data (N_B): $d = 1 - \frac{s \cdot N_C}{N_B}$. The scaling factor s describes possible differences in acceptance, photon flux and target density of the carbon and butanol data.

The double polarization observable E was determined according to Eq. (2) separately for both decay modes. Since the results were in agreement within the statistical error bars, they were combined weighted with the according errors (see Fig. 2, left).The results for the double polarization observable E as a function of the beam energy E_γ for the entire angular range $-1 \leq \cos\theta_{\eta'} \leq +1$ indicate that the contributing resonances favor the $\mathrm{A}_{1/2}$ helicity amplitude when being excited.

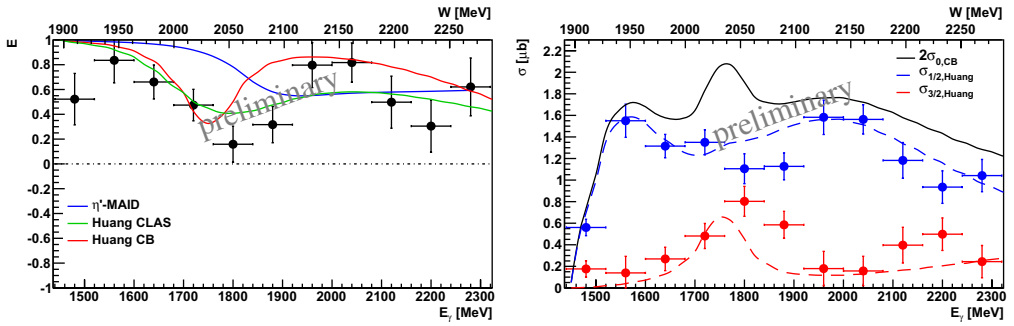

Figure 2. The double polarization observable E as a function of the beam energy (black points) together with predictions from Tiator et al. (η'-MAID) [7] and Huang et al. [6]. (Right) The helicity dependent cross sections $\sigma_{1/2}$ (blue points) and $\sigma_{3/2}$ (red points) with predictions of Huang et al. (dashed lines) and fit to the CBELSA/TAPS cross section are plotted.

The results for the double polarization observable E were further utilized to decompose the total cross section into its two helicity components $\sigma_{1/2}$ and $\sigma_{3/2}$, following Eq. (1) (compare Fig. 2, right). For $\sigma_{1/2} + \sigma_{3/2} = 2\sigma_{tot}$, the total cross section from Huang et al.'s fit to the CBELSA/TAPS data was used [6]. The helicity dependent cross sections reveal completely different structures. In $\sigma_{1/2}$, there are two peaks visible at W $\approx$ 1940 MeV and W $\approx$ 2130 MeV, which do not seem to contribute much to $\sigma_{3/2}$. According to Huang et al.'s model, these two peaks can be assigned to the $S_{11}(1925)$ and the $P_{11}(2130)$ resonances. The η'-MAID model suggests similar contributions with the $S_{11}(1904)$ and the $P_{11}(2083)$ resonances. In $\sigma_{3/2}$ however, two peaks are observed at W $\approx$ 2050 MeV and W $\approx$ 2230 MeV. Thus, resonances with total angular momentum J $= 3/2$ or higher must contribute in these mass regions. While Huang et al. believe the $P_{13}(2050)$ resonance to be involved, the η'-MAID model predicts the $D_{13}(2100)$ resonance to be responsible for the observed structure in the cross section. To decide between the different PWA-predictions additional polarization observables have to be measured.

5. Summary

The double polarization observable E has been determined for the first time in η'-photoproduction at the CBELSA/TAPS collaboration for an energy range of 1447 MeV–2320 MeV. These preliminary results for the helicity asymmetry E are compared to theoretical interpretations which indicate an overall dominance by spin 1/2 resonances and stress the important role of η'-photoproduction regarding the investigation of high-mass resonances.

This work was supported by the Deutsche Forschungsgemeinschaft (DFG) within the SFB/TR16 and the European Community-Research Infrastructure Activity (FP6).

References

[1] U. Loering et al., Eur. Phys. J. A**10**, 447-486 (2001)
[2] R.G. Edwards et al., Phys. Rev. D **84**, 074508 (2011)
[3] V. Crede et al., Phys. Rev. C **80**, 055202 (2009)
[4] M. Dugger et al., Phys. Rev. Lett. **96**, 062001 (2006)
[5] W. Chiang, F. Tabakin, Phys. Rev. C **55**, 2054 (1997)
[6] F. Huang et al., arXiv:1208.2279v1
[7] L. Tiator, Int. J. Mod. Phys. A **22**, 297-304 (2007)